Available online at www.sciencedirect.com
SCIENCE DIRECT®
PERGAMON
International Journal of Impact Engineering 30 (2004) 55–68
INTERNATIONAL JOURNAL OF IMPACT ENGINEERING
www.elsevier.com/locate/ijimpeng

Protection capability of dual flying plates against obliquely impacting long-rod penetrators

Yo-Han Yoo*, Hyunho Shin

Ground Systems Development Centre, Agency for Defence Development, P.O. Box 35-1, Daejeon 305-600, South Korea

Received 25 June 2002; received in revised form 15 April 2003

Abstract

The protection capability of dual steel flying plates against obliquely impacting tungsten heavy alloy long-rod penetrators was simulated using NET3D code. The major variables considered in this work include thickness ratios of front to rear plate (5/0, 3.3/1.7, 2.5/2.5, 1.7/3.3, and 0/5) and plate velocity (0.2 and 0.5 km/s) at obliquity of 60°. Based on the residual kinetic energy of the penetrator after perforating the plates system, the protection capability of the system increased with an increase in the ratio of rear plate thickness. Such a trend was confirmed at a normal ordnance velocity (1.5 km/s) as well as a hypervelocity regime (2.5 km/s) and was shown to be best exploited when the relative velocity between the penetrator and rear plate was appropriate. A design guideline for an effective flying plate protection structure was proposed.

Keywords: Dual flying plates; Long-rod penetrator; Oblique impact; NET3D; Explosive reactive armour

1. Introduction

Interaction phenomena between a long-rod penetrator and an oblique plate have received much attention from the viewpoint of mass efficient way of defeating the threat by introducing asymmetric loading to the penetrator. The phenomena are important in the design and performance evaluation of many types of armour systems including spaced oblique, reactive, and sensor-activated armours.

Protection capability of a stationary oblique plate against a long-rod penetrator has been the subject of many analytical works [1,2]. The physical phenomena of impact/perforation on the oblique plate have been studied in the light of ricochet/perforation criteria in the plate and

*Corresponding author.
E-mail address: yyh1986@add.re.kr (Y.-H. Yoo).

0734-743X/03/$ - see front matter
doi:10.1016/S0734-743X(03)00064-2

generation of erosion, deformation, and yaw in the residual penetrator after perforating the stationary plate [3–7]. All these combined phenomena result in an apparently enhanced protection capability of the oblique plate compared with the simple line of sight thickness of the stationary plate [8,9].

On the other hand, the analysis of the role of a flying oblique plate impacted by a long-rod penetrator has been less frequently performed while it is of interest especially in the areas of sensor-activated and reactive armours [10–12]. Lidén et al. [13] studied the impact of a long-rod penetrator onto a single oblique plate which was moving in its normal direction with a velocity component towards the incoming penetrator. Their numerical results indicate that an increase in the plate velocity does not necessarily increase the lateral disturbance on the residual penetrator. Regarding the effect of penetrator velocity, a larger penetrator disturbance was achieved by the flying plate at a higher impact velocity than that at a normal ordnance velocity.

Although useful information has been drawn in the previous works for the interaction of an obliquely impacting long-rod penetrator with a flying single plate towards the penetrator, in general, double flying plates with an explosive between the plates are considered in many explosive reactive armour systems [11]. In such cases, the oblique double plates fly away from each other in the normal direction of the plates: one plate flies with a velocity vector towards the incoming penetrator (assigned as positive direction in this work) while the other moves with a velocity component along the direction of penetrator's progress (negative direction). Consequently, the relative motion of the penetrator and the double flying plates governs the protection capability of the plates system. As the concept of the reactive armour historically started from the defeat of shaped charge jets, a number of experimental [12] and analytical [13] researches on the interaction between jet and flying plates have been performed. However, relatively less work has been performed for the case of interaction between a long-rod penetrator and dual flying plates.

For the design of a weight-efficient reactive armour system, it is important to determine an appropriate weight distribution for the two flying plates at a given total weight of the plates. Although an experimental approach offers the most accurate results for such a purpose, it is expensive and sometimes does not provide detailed information about the impact process. A computational approach can provide an insight which would be difficult to understand solely from the experimental data. This work aims to numerically investigate the effect of the weight (thickness) distribution in the dual flying plates on the protection capability against a long-rod penetrator impacting at either a normal ordnance velocity (1.5 km/s) or a hypervelocity (2.5 km/s). Another parameter studied in the present work includes the effect of the velocity of the plates moving away from each other.

2. Numerical analysis code

This work has been performed using a finite element code NET3D. The capability of NET3D in simulating other high velocity impact problems have also been published [14,15]. Some characteristic features of NET3D is described in this section.

2.1. Formulation of finite element

In order to avoid the volume locking phenomenon in standard formulation process of tetrahedral finite element, NET3D utilises velocity–pressure mixed formulation method originated by Zienkiewicz et al. [16] which treats pressure as an independent variable. Under the assumption of a constant bulk modulus, the governing equations are

$$\rho_0 \frac{\partial v_i}{\partial t} - \frac{\partial \tau_{ij}}{\partial x_j} + \frac{\partial P}{\partial x_i} = 0, \tag{1}$$

$$\frac{1}{c^2}\frac{\partial P}{\partial t} + \rho_0 \frac{\partial v_i}{\partial x_i} = 0, \tag{2}$$

where τ_{ij} is the deviatoric stress, P the pressure, v the velocity, ρ_0 the density, and c the bulk sound velocity. Above equations are momentum and mass conservation equations in i direction, respectively. The velocity–pressure mixed formulation method splits the equation using operator splitting process. In this method, temporary interim velocity is first calculated by omitting the pressure (third) term in Eq. (1). The pressure value is obtained from Eq. (2) using the interim velocity. Final velocity is then determined from Eq. (1) using the obtained pressure and the interim velocity [16,17].

2.2. Stress rate and stress update

An objective stress rate has to be used in the constitutive model instead of material time derivative since all physical quantities in constitutive equation have to maintain their objectivity. NET3D utilises Green-Naghdi stress rate for the objectivity [18]. For the polar decomposition and stress update algorithm, the method by Taylor and Flannagan [19] has been used.

2.3. Contact algorithm

The treatment of contact is largely divided into search of contact pair and calculation of contact force. The position code algorithm [20] and bucket sorting algorithm has been adopted for the contact pair search and the modified defence node algorithm for the contact force calculation [21].

3. Analysis procedure

3.1. Model geometry

The impact processes involved in reactive armours are complicated as they usually utilise an explosive: in general, plates move with a velocity gradient in time and are distorted before interacting with the incoming penetrator. In this work, an elementary case of flying dual steel plates has been considered in which a plane, i.e., un-distorted plate encounters the penetrator at a constant velocity at 60° obliquity. The cylindrical tungsten heavy alloy penetrator considered in this work was 5 mm in diameter and 75 mm in length and the steel target plates were 50 mm in width and 300 mm in length. Only half of these geometries have been modelled in three dimension

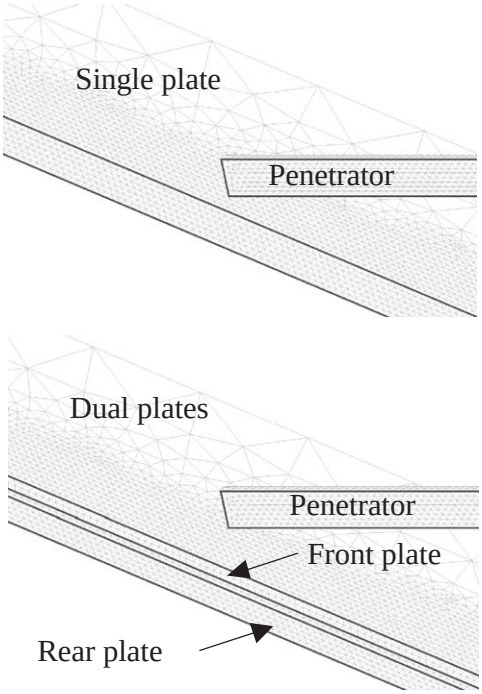

Fig. 1. Three-dimensional view of the geometry and meshes of materials modelled in this work.

due to the inherent symmetry as shown in Fig. 1. The initial gap between the two plates were 1 mm. The thickness ratios of front to rear plate were: 5/0, 3.3/1.7, 2.5/2.5, 1.7/3.3, and 0/5 under the constraint that total (front plus rear) thickness of the dual plates was 5 mm. The impact velocities considered in this work were a normal ordnance velocity (1.5 km/s) and a hypervelocity regime (2.5 km/s). The considered velocities[1] of the two plates flying away from each other were 0.2 and 0.5 km/s. Combining the impact parameters, i.e., plate thickness ratios (denoted as PT in this work), plate velocities ($V_{pl} = 0.2$ and 0.5 km/s), and penetrator velocities ($V_{pn} = 1.5$ and 2.5 km/s), 15 cases have been simulated in this work as summarized in Table 1.

3.2. Material modelling

In order to consider strain rate hardening as well as thermal softening in addition to the strain hardening considered in static deformation of metallic materials, the Jonson-Cook model [23] has been used.

$$\sigma = (A + B\varepsilon^n)\left(1 + C\ln\frac{\dot{\varepsilon}}{\dot{\varepsilon}_0}\right)\left[1 - \left(\frac{T - T_{ref}}{T_{melt} - T_{ref}}\right)^m\right]. \quad (3)$$

[1] The same magnitude of velocities (scalar) have been assumed for the dual plates in this work while in reality the plate velocity is inversely proportional to the thickness of the plates at a given amount of explosive between the plates [22]. Consequence of this assumption is discussed in Section 5.1.

Table 1
Modelling conditions for computations

Analysis groups	Velocity of penetrator V_{pn} (km/s)	Velocity of plate V_{pl} (km/s)	Run No.	Plate thickness PT, front + rear (mm)
Analysis group A	1.5	0.2	1	5 + 0
			2	3.3 + 1.7
			3	2.5 + 2.5
			4	1.7 + 3.3
			5	0 + 5
Analysis group B	1.5	0.5	6	5 + 0
			7	3.3 + 1.7
			8	2.5 + 2.5
			9	1.7 + 3.3
			10	0 + 5
Analysis group C	2.5	0.5	11	5 + 0
			12	3.3 + 1.7
			13	2.5 + 2.5
			14	1.7 + 3.3
			15	0 + 5

Table 2
Material constants for Johnson-Cook model

Material	Density (kg/m^3)	A (Gpa)	B (Gpa)	n	C	m	T_{ref} [K]	T_{melt} [K]
SIS 2541-03	7870	0.75	1.15	0.49	0.014	1.0	293	1700
DX2HCMF	17600	1.05	0.177	0.12	0.0275	1.0	293	1723

In Eq. (3), σ is the flow stress, A the static yield strength, B the strain hardening parameter, ε the equivalent plastic strain, n the strain hardening exponent, C the strain rate parameter, $\dot{\varepsilon}$ the equivalent plastic strain rate, $\dot{\varepsilon}_0$ the reference strain rate, T the temperature, T_{ref} the reference temperature, T_{melt} the melting temperature, and m the temperature exponent. The constants A, B, n, C, m and T_{melt} are determined by the material properties.

In this work, tensile failure criteria has not been set up for the metallic materials while the erosion of the finite element has been considered when equivalent plastic strain reaches 1.5. The material properties for steel (SIS 2541-03) and tungsten heavy alloy (DX2HCMF) used in the model are summarized in Table 2 following the relevant literature [13].

4. Results

Fig. 2 shows deformed shapes of the penetrators and target plates taken at 100 μs for the analysis groups A ($V_{pn} = 1.5$ km/s, $V_{pl} = 0.2$ km/s), B ($V_{pn} = 1.5$ km/s, $V_{pl} = 0.5$ km/s), and C

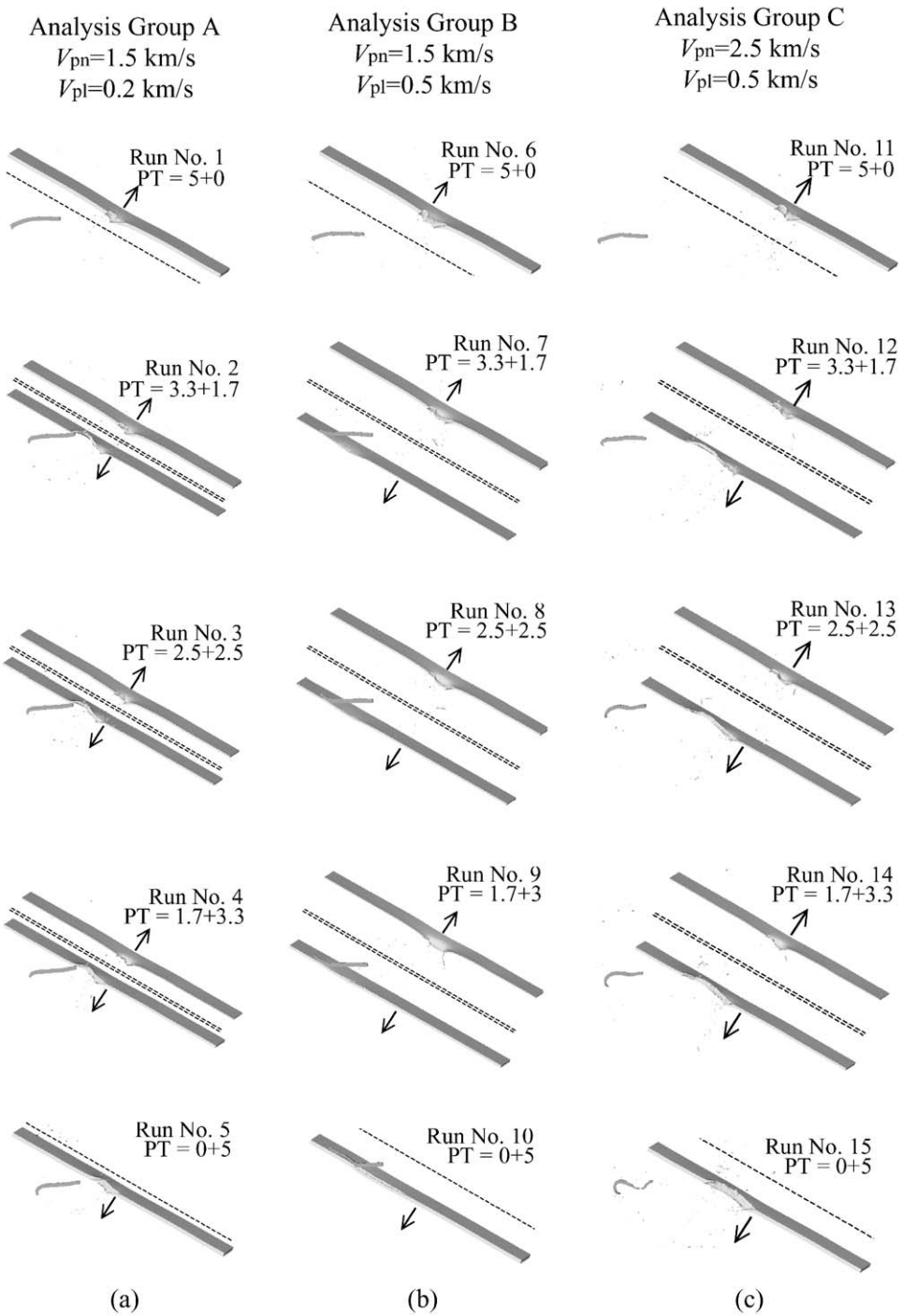

Fig. 2. Deformed shapes of the residual penetrators and plates for analysis groups (a) A, (b) B, and (c) C at 100 μs.

($V_{pn} = 2.5\,km/s$, $V_{pl} = 0.5\,km/s$) shown in Table 1. The dotted lines in the figure indicate the initial positions of the plates and the arrows represent the moving directions of the plates. The penetrator moves from right to the left direction in all the cases. All the considered cases in analysis groups A (Fig. 2(a)) and C (Fig. 2(c)) show the deformed shapes of the residual penetrators after perforating the dual plates system while the cases in analysis group B show that the penetrators are not perforating the rear plates except Run No. 6. Note that the deformed shapes of the penetrators in Fig. 2 are affected much by the change in weight (thickness) distribution in the plates (when compared in the same group), plate velocity (from comparison of groups A and B), and penetrator velocity (when groups B and C are compared).

Fig. 3 shows the change in velocity of head portion of the penetrator for the three analysis groups. In Fig. 3, the velocity initially drops at about 18 μs due to the first impact with the front plate and the behaviour thereafter is different for the cases within the analysis group as well as among different groups. In Fig. 3, the initial drop times are slightly different depending on the simulation conditions i.e., the difference in the initial gap between the penetrator and the front

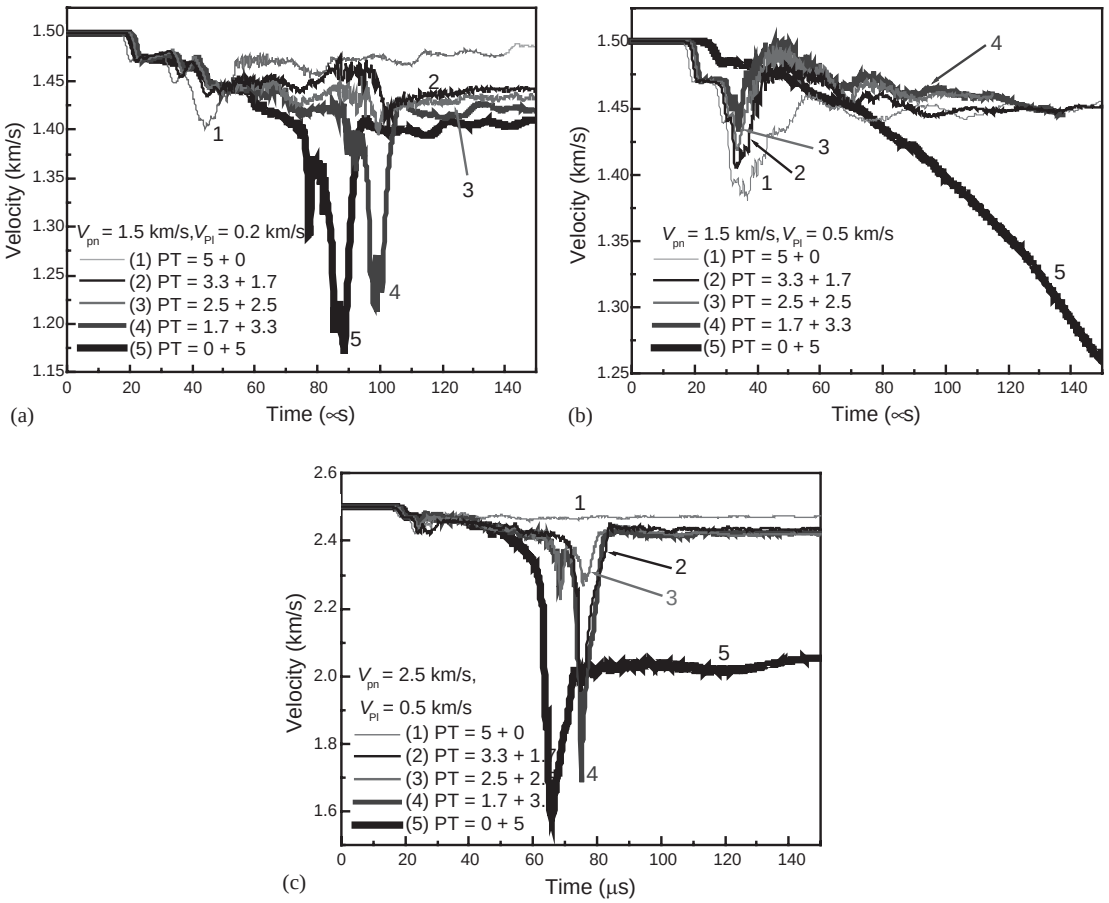

Fig. 3. Change in velocity of head portion of the penetrator for each case in analysis groups (a) A, (b) B, and (c) C.

plate, direction and velocity of the plate. Downward peaks in the figure are associated with the perforation process of the target plates.

5. Discussion

5.1. Effect of weight distribution in dual flying plates

From the deformed shapes of the penetrators in analysis groups A and C (Figs. 2(a) and (c), respectively) where the penetrator perforated the plate, it is noted that the erosion and deformation of the head portion of the residual penetrators increase apparently as the thickness of the rear plate increases while the overall bending is dominant when all the plate mass is applied to the front plate only (Run Nos. 1 and 11).

For a quantitative analysis of the residual penetration power for the cases when the penetrator perforated the dual target plates (groups A and C), the length, velocity, and effective kinetic energy of the residual penetrator has been determined as follows. When judging the protection capability of the flying plates system from the viewpoint of the residual depth of penetration (DOP) in an imaginary witness block after perforating the plates, the residual length of the penetrator only in the direction of flight is important. For instance, in case the head portion of the residual penetrator is crooked like the ones in the results of Run Nos. 5 and 15 shown in Figs. 2(a) and (c), respectively, the straight line distance, instead of the total length along the crooked head portion of the penetrator, would count for the residual DOP into the imaginary witness block. Such an effective residual length L of each penetrator has been estimated by measuring the distance between appropriate node points. The determined effective residual length L/L_0, where L_0 is the initial length of the penetrator, is shown in Fig. 4 as a function of the weight (thickness) distribution in dual plates. The residual velocity of the penetrator V has also been obtained from the time history plot in Fig. 3 at 150 μs, and the normalized result with respect to V_0, the initial velocity of the penetrator, is also shown in Fig. 4. Finally, Fig. 4 shows the change in ratio of the residual kinetic energy E to the initial value, E_0, which has been determined by[2]

$$\frac{E}{E_0} = \left(\frac{L}{L_0}\right)\left(\frac{V}{V_0}\right)^2. \tag{4}$$

As shown in Fig. 4, reduction in the penetrator length is more severe than that in velocity for the two analysis groups (A and C). The effective kinetic energy has a decreasing tendency as more fraction of weight is applied to the rear plate in both analysis groups. This indicates that the role of the rear plate is more important than the front plate in diminishing the penetration power of the penetrator. Since the relative impact velocity onto the backward-moving plate is smaller than that onto a forward-moving one, the interaction time with the penetrator is longer for the rear plate. In Figs. 3(a) and (c) in which the plate perforation takes place, there is a tendency that the intensity of the negative peaks and the reduction in velocity $V_0 - V$ thereafter increase with

[2] Apparently the residual DOP is also dependent on yaw and material integrity of the penetrator while only the effective length and velocity have been counted in this work for comparison purposes among the cases in Fig. 2. This may underestimate the effect of yaw.

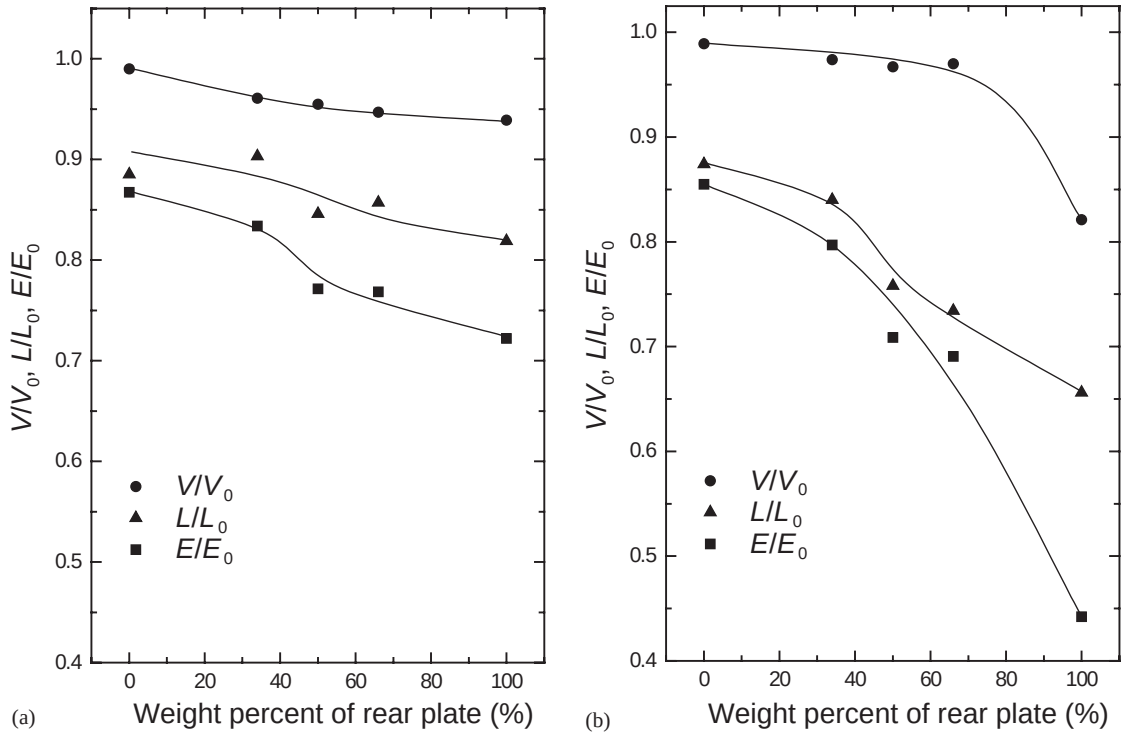

Fig. 4. Change in length ratio (L/L_0), velocity ratio (V/V_0), and kinetic energy of penetrators (E/E_0) as a function of weight fraction of the rear plate for analysis groups (a) A ($V_{pn} = 1.5$ km/s, $V_{pl} = 0.2$ km/s) and (b) C ($V_{pn} = 2.5$ km/s, $V_{pl} = 0.5$ km/s).

increase in thickness of the rear plate implying an efficient interaction between the penetrator and the plate. Hence it is deduced that the longer interaction period of time for the backward-moving plate would endow an efficient erosion/deformation and velocity reduction to the residual penetrator. Since the increase in protection capability with rear plate thickness is observed in both of the two different analysis groups A and C which have different impact conditions including two significantly different impact velocities (1.5 and 2.5 km/s), it is proposed that assigning maximal allowable mass to the rear plate would be desirable for the design of a mass-efficient plates system provided the space for the rear plate motion is allowed.

This work has been carried out under a simple assumption that the two plates have the same flying velocity regardless of their thickness as aforementioned. In a separate work by the same authors [24], a fast moving (front) plate towards the incoming penetrator showed an inferior protection capability as compared with a stationary plate. This implies that a further consideration of an increased velocity for a thinner front plate than the rear plate would not increase the protection capability of dual plates system. Therefore, the consideration of asymmetric plate velocities depending on their thickness would not seriously change the conclusion that the rear plate contributes more to the protection capability than the front one. The importance of the rear plate in defeating a long-rod penetrator is also reported in Ref. [25].

Although the type of the penetrator and plates are different, the importance of rear plate in the protection of a jet by thin (about 2 mm) plates is also addressed in literature [26].

This work used some quantitative measures of the disturbance in penetrator, such as L/L_0, V/V_0 and E/E_0, to investigate the efficiency of the plates system in reducing penetration power. It would be better to estimate the DOP in the witness block from the measures of the disturbance. However, we doubt that these measures would provide accurate DOP. We may be able to calculate the DOP in the witness block at a given distance behind the two plates system at an increased computational expense. However, the trend in DOP with respect to the weight ratio of the plates may not be generalised since the calculated DOP is strongly dependent on the distance between the witness block and the plates system due to the rotation of penetrator after perforation. Thus it would be informative to use the quantitative measures of the disturbance in Fig. 4 as parameters to draw the conclusion that assigning more weight to the rear plate is beneficial in reducing penetration power.

5.2. *Effect of flying velocity of dual plates*

Comparing the deformed shape of the penetrator of Run No. 6 with Run No. 1 in Fig. 2, in which all the plate mass is assigned to the front plate, it is noticed that the lateral erosion of the penetrator is more pronounced when the plate velocity is increased from 0.2 to 0.5 km/s. When the other cases of the weight distribution in Fig. 2(b) (Run Nos. 7–10) are compared with corresponding cases in Fig. 2(a) (Run Nos. 2–5), the increase in plate velocity from 0.2 to 0.5 km/s results in a perfect protection of the penetrator by the rear plate. The impacting penetrators in Run Nos. 7–10 are bent in such a way that the tip end is sliding parallel to the rear plate surface while the tail end remains in its impact direction (formation of a hinge). In Fig. 2(b), the length of the hinged head portion of the penetrator decreases as the thickness of the front plate increases, resulting in the increased length of the unhinged rear portion of the penetrator at the same lapse of time, i.e., 100 μs. This is because the penetrator expenses more time and energy as it perforates a thicker front plate. Although not shown in Fig. 2(b), impact features at later times indicates that the rear portion of the rod eventually passes through the point of bending while the hinge point itself moves along the plate surface. When these impact features are compared with the corresponding cases in Fig. 2(a) ($V_{\mathrm{pl}} = 0.2$ km/s), indeed, the increased backward velocity of the rear plate is yielding a ricochet (which is defined as the rebound of a striker from the impacted surface or penetration into a medium along a curved trajectory emerging through the impacted surface with a reduced velocity [27]). When the ricochet is occurring from a stationary plate, the hinge point is fixed in space [5]. However, the hinge point in this work was also travelling parallel to the target plate when $V_{\mathrm{pl}} = -0.5$ km/s because the plate has the backward-moving velocity component. The movement of the hinge point in space and the reduced relative impact velocity due to the negative plate velocity are probably responsible for the generation of the ricochet at such a low obliquity angle, i.e., 60° as compared with the stationary plate [28].

In the non-perforating cases in Fig. 2(b) (Run Nos. 7–10), the incoming penetrator is perfectly prevented from continuing its original flight. However, in case the length of the flying plates (300 mm in this work) are smaller, the remaining tail portion of the ricocheted penetrator would keep its original flight direction after reaching the end of the plate to result in a residual depth of penentration in an imaginary witness block behind the plates system. This means that the

penetration power of the ricocheted penetrator in Fig. 2(b) is system dependent, i.e., is dependent on the size of the plate, and thus the analysis shown in Fig. 4 has not been performed for the analysis group B.

6. Summary and conclusions

The protection capability of dual steel flying plates against an obliquely impacting tungsten heavy alloy long-rod penetrator was simulated using NET3D code at plate velocities of 0.2 and 0.5 km/s and the effect of weight distribution in dual flying plates on protection capability has been discovered. Based on the residual kinetic energy of the penetrator after perforating the plates system, the protection capability of the system increased with an increase in the ratio of rear plate thickness. Such a trend was confirmed at a normal ordnance velocity (1.5 km/s) as well as a hypervelocity regime (2.5 km/s) and was shown to be best exploited when the relative velocity between the penetrator and rear plate was appropriate by controlling the plate velocity. It was proposed that assigning maximal allowable weight to the rear plate would be desirable for the design of a mass-efficient protection system provided the space for the rear plate motion is allowed.

Appendix. Verification of the NET3D Simulation

In order to verify the reliability of the NET3D numerical results in this work, an experimental (flash X-ray) and numerical (AUTODYN3D) work of Lidén et al. [13] on the impact of a tungsten

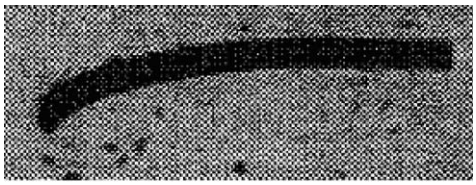

(a) Experiment (Flash X-Ray)

(b) AUTODYN3D

(c) NET3D

Fig. 5. Comparison of residual penetrators after perforating a stationary plate at impact velocity of 1.5 km/s (at 150 μs). (a) Experimentally observed shape [13], (b) simulated result by AUTODYN3D [13] and (c) result by NET3D simulation.

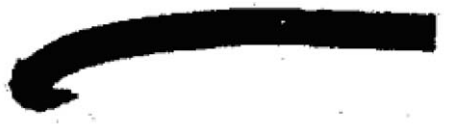

(a) AUTODYN3D

(b) NET3D

Fig. 6. Comparison of residual penetrators after perforating a stationary plate at impact velocity of 2.5 km/s (at 150 μs). (a) Result by AUTODYN3D simulation [13] and (b) by NET3D simulation.

Table 3
Results of experiments [13], AUTODYN3D [13] simulations and NET3D simulations

Impact velocity (km/s)	Residual length (L/L_0)			Residual velocity (V/V_0)			Angular velocity ($10^{3\circ}$/s)		
	Experiment	AUTO-DYN3D	NET3D	Experiment	AUTO-DYN3D	NET3D	Experiment	AUTO-DYN3D	NET3D
1.5	0.85	0.88	0.85	0.97	0.98	0.98	80	40	68
2.5	—	0.86	0.83	—	0.99	0.99	—	47	75

heavy alloy long-rod penetrator onto an oblique steel plate, has been simulated again using NET3D. For this purpose, the same material modelling condition as the one in the present work has been employed. Fig. 5 shows the residual deformed shape of the penetrator at 150 μs after perforating a stationary steel plate with 5 mm in thickness at impact velocity of 1.5 km/s. In Fig. 5, the simulated result of the deformed shape of the penetrator head portion by NET3D describes the experimental result fairly well. The simulation results by AUTODYN3D and NET3D, for the same impact situation but the impact velocity is 2.5 km/s, are shown in Fig. 6. From Figs. 5 and 6, there is a slight difference in the shape of the penetrator tip for the two simulation results, i.e., AUTODYN3D and NET3D. For a further comparison, velocity, length and angular velocity of the residual penetrator are shown in Table 3 for experimental and numerical results. From Table 3, the simulation results by NET3D appears to describe the experimental values more closely than the results of AUTODYN3D in the considered cases although there have been subtle differences in simulation criteria of the two simulations and hence the trend observed herein may not be generalised.[3] From above discussions, the simulation results in this work by NET3D do not seem to be far away from real physical phenomena.

[3] In AUTODYN3D simulation [13], the failure criterion of the plate was set up while the erosion of mesh was considered for the penetrator. Also type and size of element might be different between the two simulations.

References

[1] Yaziv D, Cox PA, Riegel III JP. Modified integral theory of impact to model long rod penetration at normal and oblique incidence. In: Schimidt SC, Dick RD, Forbes JW, Tasker DG, editors. Shock compression of condensed matter 1991. Amsterdam: Elsevier Science Publishers BV; 1992. p. 963–6.

[2] Jeanquartier R, Odermatt R. Post-perforation length and velocity of KE projectiles with single oblique targets. Proceedings of the 15th International Symposium on Ballistics, Jerusalem (Israel); 1995. p. 245–52.

[3] Holmberg L, Lundberg P, Westerling L. An experimental investigation of WHA long rods penetrating oblique steel plates. Proceedings of the 14th International Symposium on Ballistics. Quebec City (Canada); 1993. p. 515–24.

[4] Johnson W, Sengupta AK, Ghosh SK. Plasticine modelled high velocity oblique impact and ricochet of long-rods. Int J Mech Sci 1982;24(7):437–55.

[5] Senf H, Rothenhausler H. Experimental and numerical investigation of the ricocheting of projectiles from metallic surfaces. Proceedings of the 6th International Symposium on Ballistics. Orlando (USA); 1981. p. 549–60.

[6] Rosenberg Z, Yeshurun Y, Mayseless M. On the ricochet of long rod projectiles. Proceedings of the 11th International Symposium on Ballistics. Brussels (Belguim); 1989. p. 501–6.

[7] Charters AC, Menna TL, Piekutowski AJ. Penetration dynamics of rods from direct ballistic tests of advanced armor components at 2–3 km/s. Int J Impact Eng 1990;10:93–106.

[8] Yaziv D, Mayseless M, Reifen Y. The penetration process of long rods into thin metallic targets at high obliquity. Proceedings of the 19th International Symposium on Ballistics. Interlaken (Switzerland); 2001. p. 1249–55.

[9] Gee DJ. Oblique plate perforation by slender rod projectiles. Proceedings of the 19th International Symposium on Ballistics. Interlaken (Switzerland); 2001. p. 1123–32.

[10] Held M, Mayseless M, Rototaev E. Explosive reactive armour. Proceedings of the 17th international symposium on ballistics. Midrand (South Africa); 1998. p. 33–46.

[11] Held M. Disturbance of shaped charge jets by bulging armour. Propellants, Explosives, Pyrotechnics 2001;26: 191–5.

[12] Yadav HS, Kamat PV. Effect of moving plate on jet-penetration. Propellants, Explosives, Pyrotechnics 1989;14:12–8.

[13] Lidén E, Ottosson J, Holmberg L. WHA long rods penetrating stationary and moving oblique steel plates. Proceedings of the 16th International Symposium on Ballistics. San Francisco (USA); 1996. p. 703–11.

[14] Yoo Y-H, Lee M. A three dimensional FE analysis of large deformations for impact loadings using tetrahedral elements. Comput Mech 2003;30:96–105.

[15] Yoo Y-H, Chang S-N, Chung D-T. Numerical simulation of high-velocity oblique impact of mild steel spheres against mild steel plates. Trans KSME, A 2002;26(3):576–85.

[16] Zienkiewicz OC, Rojek J, Taylor RL, Pastor M. Triangles and tetrahedrals in explicit dynamic codes for solids. Int J Numer Methods Eng 1998;43:565–83.

[17] Hwang C. Three dimensional analysis of dynamic failure in high velocity impact using finite element method, Ph.D. Thesis, Seoul (Korea), Seoul National University, 2002.

[18] Johnson GC, Bammann DJ. A discussion of stress rates in finite deformation problems. Int J Solids Struct 1984;20(8):725–37.

[19] Taylor LM, Flanagan DP. Pronto2D, a two-dimensional transient solid dynamic problems Report No sand 86-0594. Albubuerque (New Mexico, USA), Sandia National Laboratories, 1987.

[20] Oldenburg M, Nilsson L. The position code algorithm for contact searching. Int J Numer Methods Eng 1994;37:359–86.

[21] Zhong ZH. Finite element procedures for contact-impact problems. London: Oxford University Press; 1993.

[22] Zukas JA, Walters WP. Explosive effects and applications. New York: Springer; 1998.

[23] Johnson GR, Cook WH. A constitutive model and data for metals subjected to large strains, high strain rates, and high temperatures. Proceedings of the 7th International Symposium on Ballistics. The Hague (Netherlands); 1983. p. 541–7.

[24] Shin H, Yoo Y-H. Effect of the velocity of a single flying plate on the protection capability against obliquely impacting long-rod penetrators. Combustion, Explosion, Shock Waves, in press.

[25] Ottosson J. A numerical study of rear plate effects, of the influence of projectile strength and geometry for a reactive armour. FOA memo 99–5523/S. 1999 (In Swedish).
[26] Ratner E. Elements for an add-on reactive armour for land vehicles. US patent No.4,741,244. 1988.
[27] Zukas JA, Gaskill B. Ricochet of deforming projectiles. Int J Impact Eng 1996;18(6):601–10.
[28] Rosenberg Z, Yeshurun Y, Mayseless M. On the ricochet of long rod projectiles. Proceedings of the 11th International Symposium on Ballistics. Brussels (Belguim); 1989. p. 501–6.